[2]Walters, R. W., and Dwoyer, D. L., "An Efficient Iteration Strategy for the Solution of the Euler Equations," *Proceedings of the AIAA 7th Computational Fluid Dynamics Conference*, AIAA, New York, 1985, pp. 381–393 (AIAA Paper 85-1529).

[3]Ying, S., and Steger, J. L., "Numerical Simulation of Unsteady, Viscous, High-Angle-of-Attack Flows Using a Partially Flux-Split Algorithm," AIAA Paper 86-2179, Aug. 1986.

[4]Newsome, R. W., Walters, R. W., and Thomas, J. L., "An Efficient Iteration Strategy for Upwind/Relaxation Solutions to the Thin-Layer Navier–Stokes Equations," *Proceedings of the AIAA 8th Computational Fluid Dynamics Conference*, AIAA, New York, 1987, pp. 126–142 (AIAA Paper 87-1113).

[5]Yoon, S., and Jameson, A., "An LU-SSSOR Scheme for the Euler and Navier–Stokes Equations," AIAA Paper 87-0600, Jan. 1987.

[6]Obayashi, S., Matsushima, K., Fujii, K., and Kuwahara, K., "Improvements in Efficiency and Reliability for Navier–Stokes Computations Using the LU-ADI Factorization Algorithm," AIAA Paper 86-0338, Jan. 1986.

[7]Pulliam, T. H., and Chaussee, D. S., "A Diagonal Form of an Implicit Approximate-Factorization Algorithm," *Journal of Computational Physics,* Vol. 39, 1977, pp. 372–397.

[8]Fujii, K., "Efficiency Improvement of Unified Implicit Relaxation/Time Integration Algorithm," *Proceedings of the AIAA 13th Computational Fluid Dynamics Conference*, AIAA, Reston, VA, 1997, pp. 161–167 (AIAA Paper 97-2105).

J. Kallinderis
Associate Editor

Numerical Study of Dynamic Stall on Several Airfoil Sections

Emmanuel Guilmineau* and Patrick Queutey*
École Centrale des Nantes, 44321 Nantes CEDEX 3, France

Introduction

THE term *dynamic stall* refers to the unsteady separation and stall phenomena of aerodynamic bodies or lifting surfaces that are forced to execute time-dependent motion, oscillatory or otherwise. It is a complex fluid dynamic phenomenon of practical importance and occurs on rapidly maneuvering aircraft, retreating helicopter rotor blades, fluttering compressor blades, and wind turbines. As summarized in extensive reviews by McCroskey[1] and Carr,[2] the unsteady flowfield generated when the airfoil reaches fairly high angles of attack during the oscillatory cycle and past the static stall angle limit is characterized by a massive unsteady separation and large-scale vortical structures. One important difference between this flowfield and that generated by the static stall is the large hysteresis in unsteady separation and reattachment of the vortex.

One reason why the flowfield associated with dynamic stall is more difficult to analyze than the static stall is its dependence on a much larger number of parameters, the most important being airfoil shape, Mach number, reduced frequency, amplitude of oscillations, type of motion (ramp or oscillatory), Reynolds number, three-dimensional effects, and wind-tunnel effects. The primary objective of the present study is to show the influence of the stall on different airfoil shapes.

Numerical Methods

The unsteady incompressible Reynolds-averaged Navier–Stokes equations (RANSE) are used to predict the stall of an airfoil. The RANSE are written in primitive formulation of the partial transformation and in a conservation form. The Cartesian velocity components and pressure share the same location at the center of the control volume. The numerical method uses a consistent physical reconstruction for the mass and momentum fluxes, the so-called consistent physical interpolation approach. This method is presented in detail by Deng et al.[3] for laminar problems and is extended to turbulent flow problems by Guilmineau et al.[4] The momentum and the continuity equations are solved in a segregated way, using the pressure implicit with splitting of operators algorithm. A second-order-accurate, three-level fully implicit time discretization is used.

In the present work, three turbulence models are used: the Baldwin–Barth (B–B) model,[5] which solves an additional equation for the turbulent Reynolds number, and both versions of the Menter K–ω model[6] [baseline version (BSL) and shear-stress transport version (SST)], which solves a first equation for the turbulent energy K and a second equation for the specific turbulent dissipation rate ω.

Results

Before presenting the results, some numerical parameters need to be specified. For each time step, a reduction of nonlinear residuals for the discrete momentum equations is required. By default, we use 10 nonlinear iterations by time step. The presented results focus on the third period of oscillations. All tests have shown that, in contrast to the findings of Raffel et al.,[7] the repeatability of calculations is good between the third cycle and those following. The oscillatory motion about the quarter-chord is defined by the time-dependent angle of attack

$$\alpha = \alpha_0 + \Delta\alpha\cos(2\pi f t) = \alpha_0 + \Delta\alpha\cos(2kt^*) \qquad (1)$$

where k is the reduced frequency, $k = 2\pi f c/2U_\infty$, and t^* the nondimensional time, $t^* = tU_\infty/c$.

All results to be presented were calculated using a 202×90 grid with a nondimensional time step of $\Delta t = 0.005$. The mesh is numerically generated by using a conformal mapping technique. The first points in fluid are located at $y^+ = 1$ away from the wall, and the outer flow boundary is located at 15 chord lengths away from the airfoil. For validation of unsteady, fully turbulent solutions, the experimental measurements[8] are used, which correspond to the deep-stall case. The Reynolds number, based on the airfoil chord length, is $Re = 10^6$. In this Note, the computations were obtained from three airfoils: the NACA 0012, the Sikorsky SC-1095, and the Vertol VR-7.

NACA 0012 Airfoil

The first considered case is that of a NACA 0012 airfoil with $\alpha_0 = 15$ deg, $\Delta\alpha = 10$ deg, and $k = 0.15$. The nondimensional period of the motion is $T^* = 20.94$. Two turbulence models have been tested: the B–B model and the SST K–ω model.

Let us consider an oscillation period starting from the minimum incidence (5 deg). As the airfoil reaches the proximity of the static stall angle ($\alpha_S \approx 12$ deg), the flowfield is still fully attached. Boundary layers on the upper surface, however, have grown considerably. Separation occurs around 20 deg. As the incidence increases, the dynamic stall vortex develops in both cases near the leading edge, although later with the K–ω model than the B–B model. This vortex is well known to be responsible for higher lift forces than those occurring at fixed incidence. At $\alpha = 23.6$ deg, the dynamic stall vortex is composed of a double structure with the B–B model. Twin eddies appear later with the K–ω model. As the airfoil incidence increases, a trailing-edge vortex is observed. At the maximum incidence, the velocity field changes drastically, and the dynamic stall vortex separates from the airfoil near the leading edge. As the trailing-edge vortex grows, the dynamic stall vortex lifts from the upper airfoil surface. This vortex takes place during a small fraction of the cycle, but its growth provokes a large oscillation lift coefficient. As the incidence decreases, the vortex core passes off the trailing edge at 24.6 deg with the K–ω model and at the maximum incidence with the B–B model. Such values can be compared with the value of 24.8 deg observed in the experimental study.[9] The shedding of the trailing-edge vortex is observed at 24.5 deg with the B–B model and at 24 deg with the K–ω model. Some secondary weak vortex structures subsequently develop. They are later shed into the wake. As the incidence decreases, the flow reattachment process starts from the leading edge downward. At $\alpha = 7.4$ deg, the reattachment of the flow occupies 60% of the chord in both turbulence models. In the experimental study,[9] it was reported that the complete reattachment occurred at $\alpha \approx 7$ deg. The evolution and the shedding of vortex

Received March 9, 1998; revision received Sept. 14, 1998; accepted for publication Sept. 16, 1998.

*CNRS Researcher, Laboratoire de Mécanique des Fluides, Centre National de la Recherche Scientifique Unité Mixte de Recherche 6598, Boite Postale 92101.

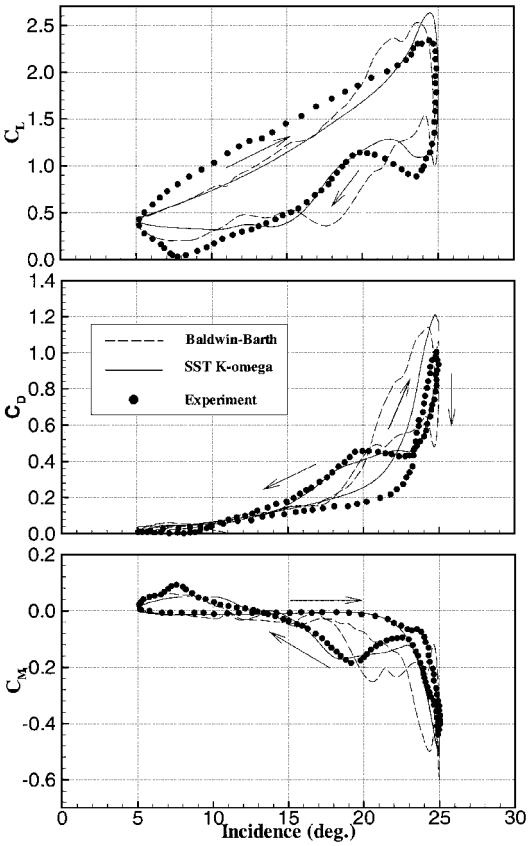

Fig. 1 Hysteresis loops, NACA 0012.

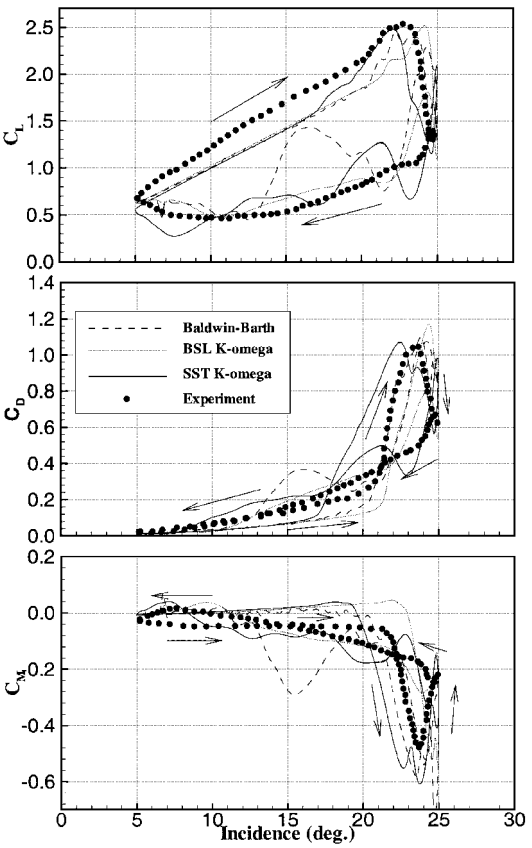

Fig. 2 Hysteresis loops, SC-1095.

predicted by the simulations with the SST $K-\omega$ turbulence model seem to be in keeping with the results of Tuncer et al.,[10] who use the Baldwin–Lomax model.

Hysteresis loops are presented in Fig. 1. Similar tends are found in both models during the upstroke phase, which shows a linear increase in the computed lift coefficient until the dynamic stall vortex reaches the trailing edge. Then the vortex suction grows, and it causes a considerable increase in lift. The computed maximum lift coefficient is overestimated with both models. The point of maximum lift defines the stall angle. Thus, the B–B model is unable to predict this angle. During the downstroke, the $K-\omega$ model gives a closer fit to experimental data[8] than the B–B model. Following the shedding of the trailing-edge vortex, the lift decreases rapidly. As the flow reattaches at the trailing edge and as the secondary vortex structures develop, the lift curve flattens. The minimum lift is observed just before the flow fully attaches to the upper surface. Similarly, the drag coefficient experiences a rapid increase with the development of the dynamic stall vortex. The time history of the moment coefficient also follows the development of the flow closely. As the leading-edge suction grows, the nose-down pitching moment increases slowly. Just as the dynamic stall vortex is shed, the moment coefficient is minimum. As the moment stall recovers, the trailing-edge vortex formation causes another indentation along the return cycle about 20 deg downward. It is then driven to its maximum value at $\alpha = 10$ deg. At this point, the flow terminates its reattachment along the upper surface. For all aerodynamic coefficients, the results with the $K-\omega$ model give a closer fit to experimental data than those of Tuncer et al.[10]

Sikorsky SC-1095 Airfoil

The second case is a Sikorsky SC-1095 airfoil. The oscillatory motion is defined by $\alpha_0 = 15$ deg, $\Delta\alpha = 10$ deg, and $k = 0.1$. The nondimensional period of the motion is $T^* = 31.415$. Three turbulence models have been tested: the B–B model, the BSL $K-\omega$ model, and the SST $K-\omega$ model.

Figure 2 presents the unsteady airloads calculated with different turbulence models. The first conclusion is that the B–B model gives fluctuations. Similarly for the NACA 0012 airfoil, during the upstroke, the lift is underpredicted with all three of the turbulence models. None of the three models predict the stall angle. The maximum lift coefficient is superior to that of the earlier case. The downstroke is not predicted correctly by any of the three models, in particular the B–B model. For the drag coefficient, the rapid increase, corresponding to the development of the dynamic stall vortex, is unestimated. The maximum drag coefficient value is slightly superior to that of the NACA 0012 airfoil. During the upstroke, the moment coefficient shows a plateau in the data. This plateau is overpredicted.

The mean-flow streamlines at the maximum incidence $\alpha = 25$ deg (not shown) present different features according to the turbulence models used. With the SST $K-\omega$ model, the leading-edge vortex spreads over the upper surface. A trailing-edge vortex exists with both remaining models; with the B–B model, it is shed. The leading-edge vortex does not have the same structure as the B–B model and the BSL $K-\omega$ model. With the $K-\omega$ model, the leading-edge eddy is composed of a double structure.

Vertol VR-7 Airfoil

We now turn to the case of Vertol VR-7 airfoil pitching. The pitching motion is defined by $\alpha_0 = 15$ deg, $\Delta\alpha = 10$ deg, and $k = 0.1$. The turbulence models used are those in the preceding case.

The hysteresis loops obtained from computations with the different turbulence models are compared with the experiment in Fig. 3. The lift coefficient is underestimated with all models during the upstroke, and the stall angle is overestimated, particularly with the B–B model and the BSL $K-\omega$ model. The SST $K-\omega$ gives a good computed maximum lift coefficient, whereas the BSL $K-\omega$ model overestimates it, and with the B–B model it is extremely underestimated. This value is similar to these found for the Sikorsky SC-1095 airfoil. The downstroke is not correctly predicted by any of the turbulence models. We obtain a trailing-edge vortex shedding that introduces a change of curve more or less early, depending on the turbulence model used. The plateau at the end of the downstroke is found only with the B–B model. For the drag coefficient the upstroke is not correctly predicted with any of the three turbulence models.

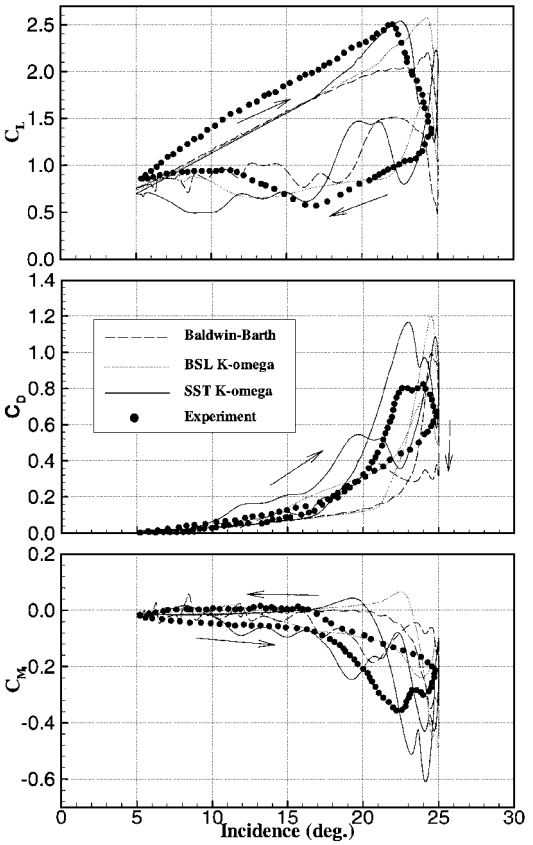

Fig. 3 Hysteresis loops, VR-7.

Its computed maximum value is overestimated with all models. This experimental value is extremely inferior to those found for the preceding case. The negative damping of the computed moment coefficient found with all of the turbulence models does not exist in the experimental data. None of the models give results that correspond to experimental data. The minimum experimental moment coefficient is -0.37 as for the Sikorsky SC-1095; this value is -0.49, and for the NACA 0012 it is -0.45. Therefore, this is the weaker minimum.

Instantaneous streamline pictures are used only for qualitative comparison of different turbulence models. For all airfoil shapes used, with the SST $K-\omega$ model turbulence model, the leading edge vortex spreads over the upper surface. With a NACA 0012 airfoil or a VR-7 airfoil, a trailing-edge vortex exists and the leading-edge vortex begins to shed. The BSL $K-\omega$ model predicts a trailing-edge eddy on the SC-1095 and VR-7 airfoils.

The flow difference between both airfoil shapes is the leading-edge vortex structure. On the SC-1095 airfoil, it is composed of a double structure. A trailing-edge eddy is predicted with the B–B turbulence model. On the SC-1095 airfoil, it is shed. The leading-edge vortex is composed of the same structure on the NACA 0012 and VR-7 airfoils.

Conclusions

The unsteady two-dimensional flowfield of an oscillating airfoil is calculated with the intention of evaluating the ability of one- and two-equation turbulence models to predict the unsteady separated flows of dynamic stall. Several airfoil shapes are used. For all test cases, the lift hysteresis, predicted by all turbulence models, is underestimated during the upstroke. The B–B model performs poorly in predicting pitching moment for all airfoil shapes. A difference exists between results given by the BSL and SST $K-\omega$ turbulence models, but neither model can be qualified as better than the other.

Acknowledgments

The authors gratefully acknowledge the Scientific Committee of the Institut du Développement et des Ressources en Informatique Scientifique du Centre National de la Recherche Scientifique (IDRIS) (Projects 96.0129 and 97.0129) for the use of CPU time on the IDRIS Cray 98.

References

[1]McCroskey, W. J., "The Phenomenon of Dynamic Stall," NASA TM-81264, March 1981.

[2]Carr, L. W., "Progress in Analysis and Prediction of Dynamic Stall," *Journal of Aircraft*, Vol. 25, No. 1, 1988, pp. 6–17.

[3]Deng, G. B., Guilmineau, E., Piquet, J., Queutey, P., and Visonneau, M., "Computation of Unsteady Laminar Viscous Flow Past an Aerofoil," *International Journal for Numerical Methods in Fluids*, Vol. 19, No. 9, 1994, pp. 765–794.

[4]Guilmineau, E., Piquet, J., and Queutey, P., "Two-Dimensional Turbulent Viscous Flow Simulation Past Airfoils at Fixed Incidence," *Computers and Fluids*, Vol. 26, No. 2, 1997, pp. 135–162

[5]Baldwin, B. S., and Barth, T. J., "A One-Equation Turbulence Transport Model for High Reynolds Number Wall-Bounded Flows," AIAA Paper 91-0610, Jan. 1991.

[6]Menter, F. R., "Zonal Two-Equation $K-\omega$ Turbulence Models for Aerodynamic Flows," AIAA Paper 93-2906, July 1993.

[7]Raffel, M., Kompenhans, J., and Wernert, P., "Investigation of the Unsteady Flow Velocity Field Above an Airfoil Pitching Under Deep Dynamic Stall Conditions," *Experiments in Fluids*, Vol. 19, 1995, pp. 103–111.

[8]McAlister, K. W., Pucci, S. L., McCroskey, W. J., and Carr, L. W., "An Experimental Study of Dynamic Stall on Advanced Airfoil Sections, Pressure and Force Data," NASA TM-84245, Dec. 1982.

[9]Carr, L. W., McAlister, K. W., and McCroskey, W. J., "Analysis of the Development of Dynamic Stall Based on Oscillating Airfoil Experiments," NASA TN-D-8382, Jan. 1977.

[10]Tuncer, I. H., Wu, J. C., and Wang, C. M., "Theorical and Numerical Studies of Oscillating Airfoils," *AIAA Journal*, Vol. 28, No. 9, 1990, pp. 1615–1624.

A. Plotkin
Associate Editor

Flowfield Measurements over an Airfoil During Natural Low-Frequency Oscillations near Stall

A. P. Broeren* and M. B. Bragg†
University of Illinois at Urbana–Champaign, Urbana, Illinois 61801

Introduction

THERE exists for flows past certain airfoils, near the onset of stall, a naturally occurring unsteady flow oscillation that is very low in frequency, with the Strouhal number typically on the order of 0.02. Here the Strouhal number is defined as $Sr = f c \sin \alpha / U_\infty$, where f is the oscillation frequency, c is the airfoil chord, α is the angle of attack, and U_∞ is the freestream speed. This low-frequency flow oscillation was studied in detail at low Reynolds numbers for an LRN(1)-1007 airfoil by Zaman et al.,[1] who concluded that the flow oscillation involved quasiperiodic switching between stalled and unstalled states. Evidence gathered from oil-flow and laser-sheet-flow visualization led Bragg et al.[2] to suggest that the unsteady stall was related to the growth and bursting of a laminar separation bubble. The oil-flow visualization also showed that the flowfield leading up to stall was two dimensional.[3]

Received May 27, 1998; revision received Sept. 19, 1998; accepted for publication Sept. 23, 1998.

*Graduate Research Assistant, Department of Mechanical and Industrial Engineering, 140 Mechanical Engineering Building, 1206 W. Green Street. Member AIAA.

†Professor, Department of Aeronautical and Astronautical Engineering, 306 Talbot Laboratory, 104 S. Wright Street. Associate Fellow AIAA.